Journal of the European Ceramic Society 40 (2020) 4655–4663

Contents lists available at ScienceDirect

Journal of the European Ceramic Society

journal homepage: www.elsevier.com/locate/jeurceramsoc

Original Article

R-curves determination of ordinary refractory ceramics assisted by digital image correlation method

Yajie Dai[a,b,*], Harald Harmuth[c], Shengli Jin[c], Dietmar Gruber[c], Yawei Li[a,b]

[a] The State Key Laboratory of Refractories and Metallurgy, Wuhan University of Science and Technology, Wuhan 430081, China
[b] National-Provincial Joint Engineering Research Center of High Temperature Materials and Lining Technology, Wuhan 430081, China
[c] Chair of Ceramics, Montanuniversität Leoben, Peter-Tunner Strasse 5, 8700 Leoben, Austria

ARTICLE INFO

Keywords:
Universal dimensionless load–displacement diagram method
R-curve
Magnesia refractories
Fracture process
Digital image correlation

ABSTRACT

As a figure-of-merit, the rising ratio of crack propagation resistance to fracture initiation resistance indicates a reduction of the brittleness and enhances the thermal shock resistance of ordinary refractory ceramics. The significant nonlinear fracture behaviour is related to the development of a fracture process zone (FPZ). The universal dimensionless load–displacement diagram method is applied as a promising graphical method for the determination of *R*-curves for magnesia refractories showing different brittleness. By applying digital image correlation (DIC) together with the graphical method, the problems arisen with accurate determination of the fracture initiation resistance and the crack length are overcome. Meanwhile, the *R*-curve is subdivided with respect to the fracture processes, viz the fracture initiation, the development of FPZ and the onset of traction free macro-crack. With the simultaneous crack lengths evaluated from DIC, the contribution of each fracture process to the crack propagation resistance at certain loading stage is quantitatively presented.

1. Introduction

The fracture behaviour of ordinary refractory ceramics is rather complicated due to its high heterogeneous porous grain/matrix structure. Most refractories do not strictly obey linear elastic fracture mechanics (LEFM) [1–3]. The thermal shock resistance, which is crucial for refractory materials serving under mechanical and thermal stresses, is closely related to the deviation from LEFM [4,5]. The R'''' parameter proposed by Hasselman serves as one of the figures-of-merit for the thermal shock resistance [6]:

$$R'''' = \frac{\gamma}{f_t^2/E} = \frac{l_{ch}}{2}. \quad (1)$$

Here γ is the specific fracture surface energy, f_t the tensile strength, E the Young's modulus and l_{ch} the characteristic length [7]. The l_{ch} can be used to define the material brittleness. The denominator *2* in Eq. (1) follows from the different definition of the fracture energy applied for R'''' and l_{ch}. For R'''', the fracture energy is divided by the double projection of the fractured cross section, while by the single one for l_{ch}. According to the definition shown in Eq. (1), R'''' is proportional to the ratio of the fracture energy for crack propagation to the stored elastic energy for crack initiation. The pronounced deviation from LEFM is favourable for achieving a refractory material with reduced brittleness and high thermal shock resistance. During the manufacture of refractory material, one of the most applied methods for reducing the brittleness is to generate the pre-existing micro-crack networks in the microstructure, e.g. via the addition of spinel grains into the matrix of a magnesia refractory [8,9].

Refractories showing reduced brittleness exhibit remarkably increasing crack propagation resistance with crack length, so-called rising *R*-curve behaviour [4,10]. The deviation from LEFM is attributed to the energy consuming processes occurring not only at the crack tip but also in the fracture process zone (both the frontal process zone and the process wake) [7,11–13]. As it is well known, the shape of *R*-curves gives an indication of material brittleness [3]. For instance, a flat *R*-curve refers to a perfect brittle linear elastic fracture, a rising *R*-curve followed with a plateau is corresponding with nonlinear fracture behaviour with the formation of a constant FPZ, and a continuously rising *R*-curve is related to a further increase of FPZ. The fracture initiation resistance as well as the slope and the plateau value of the rising *R*-curve are also essential information for understanding the fracture behaviour of refractory materials. The loading–unloading technique and the multi-specimens method (various specimens with different initial notch lengths) were commonly used for the evaluation of *R*-curve [14]. However, the results are significantly influenced by the friction in the process wake for both methods.

* Corresponding author at: The State Key Laboratory of Refractories and Metallurgy, Wuhan University of Science and Technology, Wuhan 430081, China.
E-mail address: yajie.dai@wust.edu.cn (Y. Dai).

https://doi.org/10.1016/j.jeurceramsoc.2020.05.047
Received 17 January 2020; Received in revised form 16 May 2020; Accepted 17 May 2020
Available online 20 May 2020

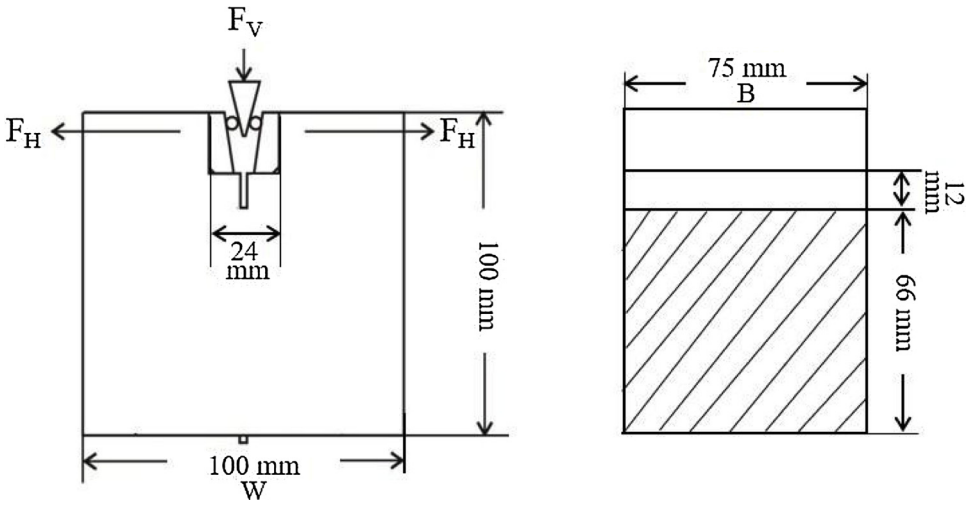

Fig. 1. Schematic representation of wedge splitting test.

Comparatively speaking, the so-called universal dimensionless load–displacement diagram technique, which was introduced by Sakai et al. [14], seems to be a promising method for determining the *R*-curves. It requires only one single specimen and no artificial unloading procedure. The *R*-curve is derived from one load–displacement curve by separating the elastic and the inelastic part of the total deformation. This technique has already been applied with the wedge spitting test for different materials [4,15,16]. There exist two difficulties for the exact determination of *R*-curve by the universal dimensionless load–displacement diagram technique. First of all, two main stages can be distinguished: development of the FPZ and further extension of the macro-crack during the fracture process of quasi-brittle materials [17–19]. The fracture initiates before reaching the maximum load for refractory materials with reduced brittleness. However, according to its principle, the universal dimensionless load–displacement diagram technique assumes the fracture initiates at the maximum load and the specimen fracture is caused by a single straight crack propagation without taking into account the detailed fracture processes and the tortuous crack path. As a result, the evaluated fracture initiation resistance and the *R*-curve cannot completely represent the actual fracture behaviour of quasi-brittle materials, particularly for those with sizable FPZ. The crack propagation resistance before reaching the maximum load is unable to be evaluated as well.

Secondly, the micro-cracking, crack branching and other micro processes causing deviations from LEFM often take place during the damage process of ordinary refractory ceramics [20,21], which result in the difficult determination of crack tip and crack length for *R*-curve evaluation. Normally, the crack length evolution was evaluated from the compliance function [22]. Furthermore, different techniques could also be used for the determination of the crack lengths, such as the ultrasonic [23], the electrical resistivity [24] and the digital image correlation (DIC) [17,18,25]. The DIC is a non-contact optical measurement technique, which evaluates the two-dimensional full-field deformation [26] and has been proven to be an efficient approach for locating the crack tip and monitoring the instantaneous crack length of different quasi-brittle materials. By coupling the DIC technique together with mechanical measurements, the fracture parameters, i.e. the stress intensity factors and the crack propagation resistance, can be studied [27–29].

In order to overcome the above-mentioned difficulties, some modifications of the universal dimensionless load–displacement diagram technique and solutions are proposed in this study. Together with DIC measurements, the determination of crack length and the influence of the fracture processes on the *R*-curve are investigated for refractory materials with different brittleness. This study helps to assess the validity of *R*-curves as determined by the universal dimensionless load–displacement diagram technique and gives new insight into the fracture behaviour of refractory materials.

2. Testing and evaluation methods

2.1. Experimental investigation

In order to investigate the relationship between the fracture process and *R*-curve behaviour, two typical refractory materials showing different brittleness were evaluated in this study: a magnesia material and a magnesia spinel material. Due to the thermal misfit between magnesia matrix and spinel grains, a micro-crack network is induced in the magnesia spinel material during manufacture. Compared with a pure magnesia material, the maximum load is thus reduced for magnesia spinel material, but further crack propagation is hindered [17]. It shows a pronounced deviation from LEFM. The wedge splitting test (WST), patented in 1986 by Tschegg [30], ensures stable crack propagation for quasi-brittle materials due to the wedge transmission and the favourable specimen shape. The load–displacement curve, specific fracture energy and nominal notch tensile strength can be determined by WST. The schematic representation and specimen geometry of WST are shown in Fig. 1. Meanwhile, a CMOS camera with a resolution of 18 Megapixels was placed in front of the specimen to successively record the digital images during the entire WST. The images were analysed by using the post-processing software MatchID 2D to evaluate the instantaneous crack length and the development of FPZ for magnesia material and magnesia spinel material. The experimental data used in this work are from the previous publication of the authors [17], where more information about the studied materials and the experimental method can been found as well.

2.2. Evaluation of the measurements

Fig. 2 exhibits the fundamental idea of the universal dimensionless load–displacement technique, which provides the nonlinear fracture parameters from one single measurement [14]. The solid curve, which represents the experimental load–displacement curve of a refractory ceramic material deviating from LEFM, is compared with that of a perfectly linear elastic material. The linear elastic case shows the same maximum load and Young's Modulus as the experimentally investigated material. In the case that crack initiation would take place at maximum load for the refractory material, both cases would also show the same critical stress intensity factor. The horizontal distance B′–B indicates the irreversible displacement at point B and the reversible displacement is

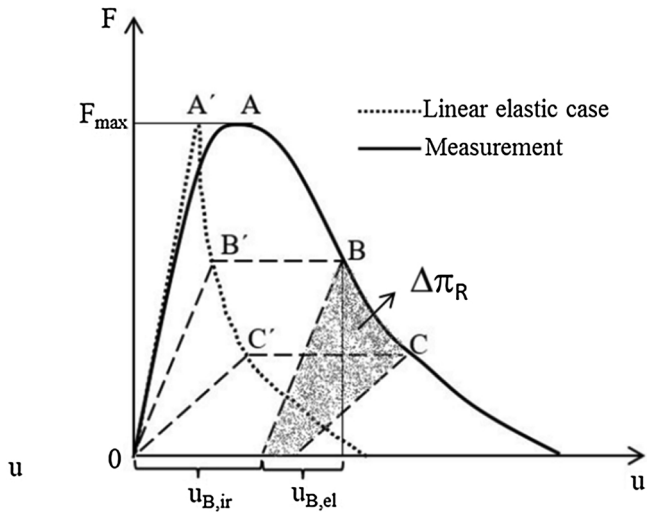

Fig. 2. Schematic illustration of the universal dimensionless load–displacement diagram technique.

shown by the linear elastic case. The inverse slope of line OB′ yields the compliance which was used to calculate the nominal crack length. The shaded area in Fig. 2 represents the irreversible energy consumption for the crack extension Δa from B to C.

Once the irreversible energy ($\Delta\pi_{R,i}$) for each crack extension (a_{i+1}-a_i) is obtained, the crack propagation resistance at each crack length can be evaluated by using Eq. (2):

$$R_{C,i} = \frac{\Delta\pi_{R,i}}{B(a_{i+1} - a_{i})}. \tag{2}$$

Dimensionless quantities for load F_r and displacement u_r are usually applied and defined as follows:

$$F_r = \frac{F_c}{K_{IC}BW^{1/2}} \tag{3}$$

$$u_r = \frac{u_c E}{K_{IC}W^{1/2}}. \tag{4}$$

Here F_c is the respective load, u_c the displacement, K_{IC} the critical stress intensity factor, B the specimen thickness and W the specimen width.

The perfect linear elastic material strictly follows the LEFM where the load is a function of K_{IC} using the crack length (a) as the variable [31]:

$$F_c = \frac{K_{IC}BW^{1/2}}{Y(a/W)} \tag{5}$$

Here $Y(a/W)$ is a dimensionless geometry function depending on crack length. Moreover, the reversible elastic displacement can be calculated from the fracture load using the specimen compliance (C) [32]:

$$u_c = \frac{\lambda(a/W)}{BE}F_c = CF_c. \tag{6}$$

Here $\lambda(a/W)$ is the dimensionless compliance.

Using Eqs (3)–(6) the dimensionless fracture load and the dimensionless displacement of a linear elastic material could be expressed by:

$$F_r = \frac{1}{Y(a/W)} \tag{7}$$

$$u_r = \frac{\lambda(a/W)}{Y(a/W)}. \tag{8}$$

According to the equations above, the dimensionless load–displacement relationship for all linear elastic materials is a single universal curve depending only on the geometry factors $Y(a/W)$ and $\lambda(a/W)$. To evaluate these two geometry factors, a series of linear elastic finite element simulations was performed using the WST geometry shown in Fig. 1. The specimen thickness and width keep constant, while the crack length varies. According to the F_c–u_c relationship of linear elastic material with different crack length, the dimensionless compliance $\lambda(a/W)$ is determined by using Eq. (6). As expected, the dimensionless compliance $\lambda(a/W)$ remarkably increases with the crack length.

According to Fett et al. [32], the dimensionless geometry factor $Y(a/W)$ can be calculated from the dimensionless compliance $\lambda(a/W)$:

$$Y(a/W) = \sqrt{\frac{1}{2}\frac{\partial\lambda(a/W)}{\partial(a/W)}}. \tag{9}$$

With the knowledge of these functions, the R_C curve can be determined successively based on the universal dimension less load–displacement technique. Besides the crack length determined from the compliance, the DIC technique was adopted simultaneously to evaluate the crack length. The detailed evaluation of FPZ and crack length for magnesia material and magnesia spinel material by DIC characterization is published elsewhere [17]; the obtained crack length will be directly used here. The evaluation of R-curve and the clarification of the influence of fracture process on the R-curve determination will be shown in the follow section.

3. Results and discussion

3.1. Analysis of fracture initiation

Fig. 4 shows the dimensionless load–displacement curves of magnesia spinel material (a) and magnesia material (b) as well as the corresponding linear elastic cases. Dimensionless quantities have been calculated according to the Eqs. (3) and (4). Moreover, the dimensionless linear elastic curves are determined with the help of the two functions obtained from the finite element simulation (Fig. 3). As seen from Fig. 4, the deviations of experimentally measured curves of refractory materials from linear elastic curves are significant.

The universal dimensionless load–displacement diagram technique assumes that the fracture of quasi-brittle material initiates at the maximum load. However, according to the DIC observation, for brittleness reduced refractory materials the development of FPZ initiates before reaching the maximum load. As for the investigated magnesia spinel refractory specimen, the fracture starts at the 82% F_{max} in the pre-peak region [17]. Contrary, the fracture initiation of the brittle pure magnesia material is detected at the maximum load. Fig. 4 exhibits three linear elastic cases: case 1 and 3 refer to a linear elastic material showing the same maximum load as the magnesia spinel material and magnesia material, respectively; case 2 indicates that the fracture of the

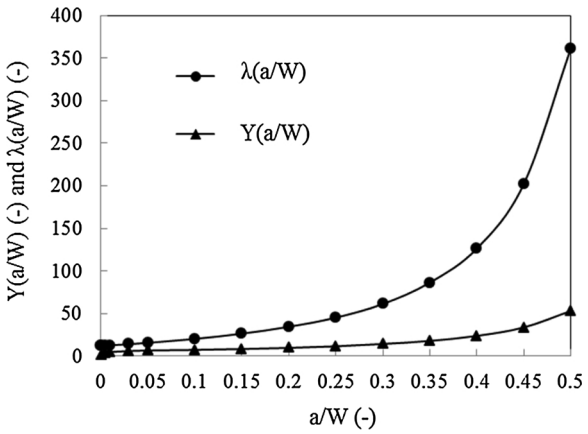

Fig. 3. Dependence of the dimensionless functions $\lambda(a/W)$ and $Y(a/W)$ on the crack length.

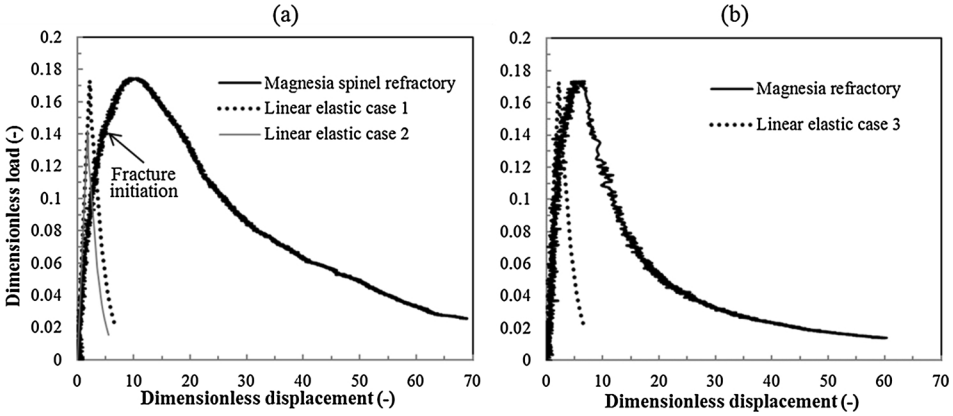

Fig. 4. Dimensionless load–displacement curves of magnesia spinel material (a) and of magnesia material (b) (solid curves: the dimensionless experimental curves [17]; dotted and grey curves: the dimensionless curves for the linear elastic cases).

linear elastic material commences at the 82% F_{max} of magnesia spinel material based on the DIC observation.

The critical stress intensity factor K_{IC} for crack initiation can be determined from the corresponding critical force $F_{critical}$:

$$K_{IC} = \frac{Y(0)}{BW^{1/2}} F_{critical} \tag{10}$$

With the assumption of plane stress, the critical energy release rate could be calculated from the K_{IC} according to Irwin [33]:

$$G_C = \frac{{K_{IC}}^2}{E}. \tag{11}$$

Eq. (11) holds for a perfectly linear elastic material only. In the regime of nonlinear elastic fracture, a generalized Irwin's similarity relationship is derived [34]:

$$R_c = \frac{{K_{IC}}^2}{E}(1 + 2\eta). \tag{12}$$

The term η, which can be considered as a measure of deviation from pure LEFM, is derivative of the irreversible displacement with respect to the elastic displacement:

$$\eta = \frac{\partial u_{ir}}{\partial u_{el}}. \tag{13}$$

This quantity can be approximated by

$$\eta \approx \frac{\Delta u_c - \Delta u_{el}}{\Delta u_{el}} \tag{14}$$

where

$$\Delta u_c = u_{c,i+1} - u_{c,i} \tag{15}$$

is the total displacement difference of two consecutive instants chosen for evaluation and the associated elastic displacement difference:

$$\Delta u_{el} = (\lambda(a_{i+1}/W)F_{c,i+1} - \lambda(a_i/W)F_{c,i})/BE. \tag{16}$$

When η equals to 0, the Eq. (12) becomes the Irwin expression.

The Young's Modulus can be obtained by resonant frequency damping analysis (RFDA) separately or calculated from the slope of the load–displacement curve in its elastic region:

$$E = \frac{dF_H}{du}\frac{\lambda(0)}{B}. \tag{17}$$

The initial dimensionless compliance $\lambda(0)$ of the WST specimen equals to 12.7 as shown in Fig. 3. All experiments have been performed at ambient temperature. The Young's Modulus of magnesia refractory and magnesia spinel refractory are 96 GPa and 21 GPa, respectively.

The parameters of fracture initiation of magnesia spinel material and magnesia material are shown in Table 1 which exhibits two cases for magnesia spinel material (case 1 and 2): fracture initiation at maximum load and at the 82% F_{max}, respectively. The K_{IC} and G_C evaluated from case 1 are higher than those obtained from case 2. Magnesia material shows higher fracture initiation resistance than magnesia spinel material. For magnesia spinel material, the critical stress intensity factor is only 30% of magnesia material, and less than half of the critical energy release rate is required for the fracture initiation.

Table 1
Parameters K_{IC} and G_C of magnesia spinel material and magnesia material.

	F_{critical} (N)	K_{IC} (MPa m$^{1/2}$)	G_C (N/m)
Linear elastic case 1	2842	0.69	22.8
Linear elastic case 2	2330	0.57	15.4
Linear elastic case 3	7934	1.93	38.9

3.2. Determination of R-curves and deviation from LEFM

The definition and determination of the crack length has a significant influence on the result of the crack propagation resistance evaluation. Here four different crack lengths will be defined and used for further investigation of the fracture behaviour of the magnesia spinel material. According to the DIC results, the fracture process of this material comprises two stages: the development of the FPZ and the subsequent extension of the traction free macro-crack. The onset of macro-crack, which takes place in the post-peak region, is indicated by the variation of the localized zone size [17]. Fig. 5 illustrates the localized zone and the macro-crack evaluated from the strain field of magnesia spinel material. With the application of DIC, the localized zone tip and macro-crack tip can be precisely located. This procedure is more detailed explained in [23]. Thus, the maximum length of localized zone L_M and the macro-crack length a_m at different loading stages are successively achieved. The evolution of L_M and a_m are shown in Fig. 6 with respect to the horizontal displacement measured at the loading points.

The nominal crack length a_n in Fig. 6 is calculated from the compliance. In the first stage of the fracture process, the energy is dissipated for the free development of FPZ. Seen from Fig. 6, once the macro-crack is onset, the extension of localized zone is limited and the rapid propagation of the macro-crack consumes large part of the energy in the second stage. The difference between the localized zone length and macro-crack length is denoted as the length of FPZ. The maximum length of FPZ reaches approximately 55 mm, which is in the same scale of the specimen geometry. This occurs at the onset of macro-crack formation. As shown in Fig. 5, the crack lengths evaluated by DIC are measured along the tortuous crack path, which is more precise than just

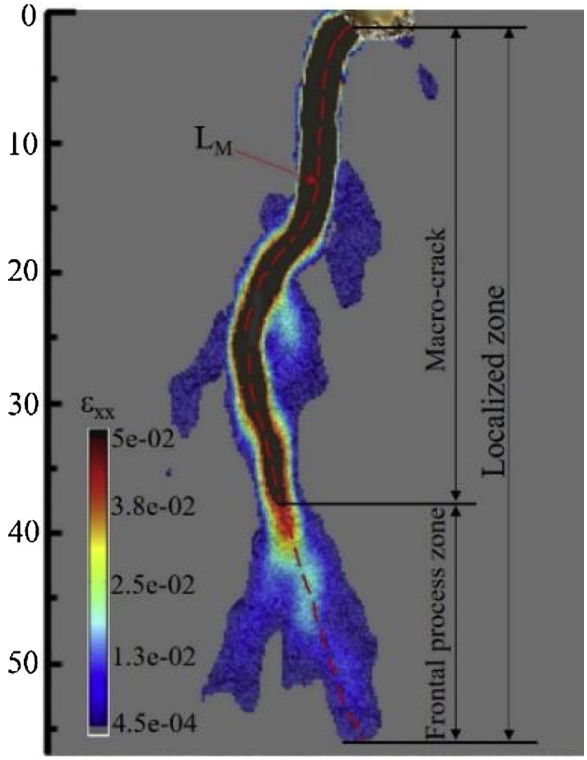

Fig. 5. Illustration of the localized zone and the macro-crack (colours represent horizontal strains ε_{xx}) [23].

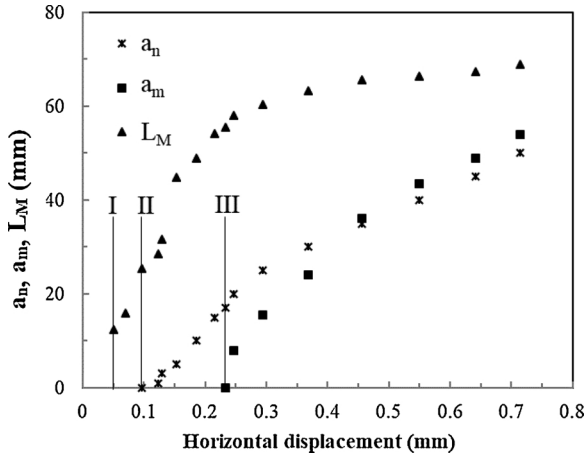

Fig. 6. Evolution of crack length for magnesia spinel material with respect to the measured horizontal displacement (I: fracture initiation in pre-peak region; II: maximum load; III: onset of macro-crack in post-peak region).

considering the linear distance between the notch and the crack tip. As shown in Fig. 6, the onset of these crack length measures is different: the localized zone initiates in the pre-peak region; the nominal crack length is assumed to start at the maximum load and the macro-crack is onset in the post-peak region.

According to Eq. (2), the crack propagation resistance can be calculated as the dissipated energy over the crack length. Fig. 7(a)exhibits the dependence of the cumulative dissipated energy on the different crack length measures introduced above. At each loading stage of magnesia spinel material, the dissipated energy is calculated as illustrated in Fig. 2 and the crack lengths are determined either from the compliance or by DIC. For a_n and a_m, the slope calculated from the origin and the first data point is very steep, which would result in extremely high crack propagation resistance at beginning. This is misleading, caused by the energy already consumed before, and does not represent a material property. The compliance method assumes the crack initiates at the maximum load. The energy consumed by the FPZ development in the pre-peak region is added and causes the relatively large value at a low crack length. Similarly, when the macro crack evolves, a large amount of the whole fracture energy was already consumed for FPZ development. If the first data points of a_n and a_m are ignored to avoid the unjustified sudden increase and followed decrease in R-curves, the results will look like as in Fig. 7(b).

The integral of R_C with respect to the crack length over the whole range of crack length has to be equal to total fracture energy per unit specimen width and therefore should be equal for all the methods. However, the integrals of obtained R-curves in Fig. 7(b) do not yield the same value due to the omission of the first data points. According to the DIC results, the dissipated energy in dependence of L_M would represent more realistically the fracture behaviour before the load peak than of a_n and before the onset of macro-crack than of a_m. In order to solve this problem, the redefinition of the crack lengths a_n and a_m are necessary:

$$a_n'(u) = \begin{cases} L_M(u)\ u < u(F_{max}) \\ L_M(u(F_{max})) + a_n(u)\ u > u(F_{max}) \end{cases} \quad (18)$$

$$a_m'(u) = \begin{cases} L_M(u)\ u < u(a_m = 0) \\ L_M(u) + a_m(u)\ u > u(a_m = 0) \end{cases} \quad (19)$$

The a_n' and a_m' are the redefined nominal crack length and macro-crack length. Before reaching the maximum load and the onset of macro-crack, the a_n' and a_m' equal to the L_M, respectively. The R_C determined with these redefined crack lengths are shown in Fig. 8: the former influence of the first data points on the results is eliminated by this new crack length definition.

As shown in Fig. 7(b), the curve given by L_M might give the impression of a large rise of the R-curve at the final stage of fracture process. Once the macro-crack is formed, R_C dependent on L_M increases significantly as the further extension of localized zone is restricted by the specimen geometry and the main energy is consumed for the macro-crack propagation that takes place at the expense of the FPZ. This means that a_m increases more than L_M which causes the significant increase of the R_C over L_M. A so-called composite crack length a_c is defined to investigate the influence of different fracture processes on the crack propagation resistance:

$$a_c = L_M + a_m. \quad (20)$$

It is important to recognize that the composite crack length is not the length of an actually occurring crack within the sample. The R_C determined by the a_c represents the influence of all fracture processes on the R-curve behaviour. In the first stage of fracture process, the macro-crack is not onset yet. Thus, a_c equals to L_M and exhibits the FPZ propagation resistance. Once the macro-crack starts, it is effective to evaluate the propagation resistance of the FPZ together with the macro-crack evolution in the second stage of fracture process. The difference between R_C determined by a_m' and a_c refers to the contribution from the L_M to the crack propagation resistance at the second fracture stage. According to the values, it is proven that in the second fracture stage, the dominant process is the propagation of the macro-crack.

By depicting R_C together with the load in dependence of the displacement, the crack propagation resistance of magnesia spinel material at different loading stages can be clearly represented. As shown in Fig. 9, the R-curves determined by compliance and by DIC, respectively, have been compared. For both methods, rising R-curves have been observed. The application of DIC supports the combined consideration of the observed fracture process together with the R-curve behaviour. The fracture of magnesia spinel material initiates in the pre-peak region; the development of FPZ increases R_C; since the onset of a macro-crack, the plateau of R-curve is achieved and the macro-crack extension dominates the resistance of crack propagation. This is shown by the R_C–a_m curve. As for R_C determined by compliance (R_C–a_n), the fracture

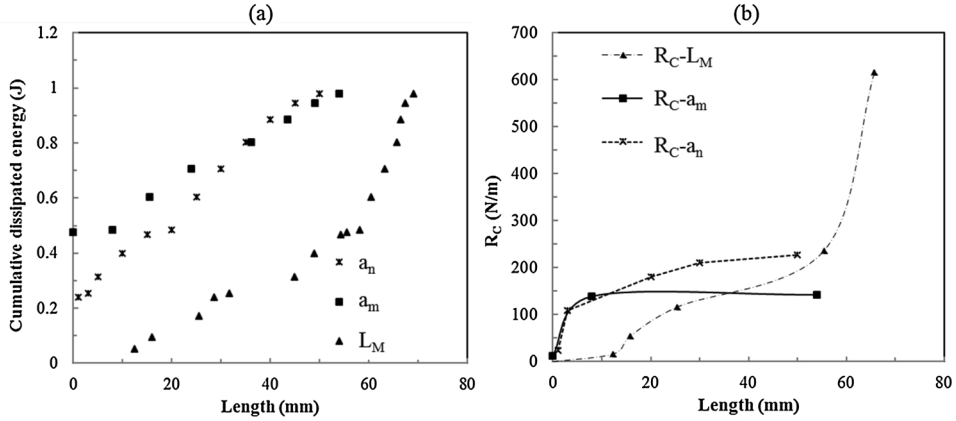

Fig. 7. Cumulative dissipated energy (a) and crack growth resistance R_C (b) for magnesia spinel material.

initiation is at the load peak which deviates from the reality of the fracture process for refractories showing reduced brittleness. The plateau value of the R_C–a_n curve, which is approximately 230 N/m, is higher than that determined by DIC. The compliance method attributes the energy consumption of all the fracture processes (i.e. crack branching, deflection of crack path) to the extension of a straight crack. However, the crack lengths measures by DIC represent a tortuous crack length and different fracture processes (FPZ and macro crack) are distinguished.

The magnesia refractory material is relatively brittle. The fracture initiates at the maximum load, which agrees with the assumption of compliance method. Moreover, as shown in Fig. 10(a), compared to the magnesia spinel material the difference between the localized zone length and the macro-crack length is smaller. This indicates that only a small FPZ is formed during the fracture process of magnesia material. For the same cumulative dissipated energy, the DIC measured crack lengths (a_m and L_M) are longer than the crack length determined by compliance. This results in higher R_C value determined by compliance as seen from Fig. 10(b). Once the crack tip reaches the bottom region of the WST specimen, the dissipated energy increases with less crack length extension, seen from the high slope at the final stage of the curves in Fig. 10(a). In order to reduce the influence of the finite specimen size, R_C is evaluated for $a_m \leq 50$ mm, while a_n amounts to 35 mm only. Fig. 10(b) shows the dependence of R_C on the horizontal displacement and on the crack length (insert). Compared with magnesia spinel material, the post-peak region of the load–displacement diagram is narrower for magnesia material and the macro-crack length extends already to 50 mm at a relatively small horizontal displacement. This verifies that the reduction of brittleness increases the strain-to-rupture of refractory materials [20].

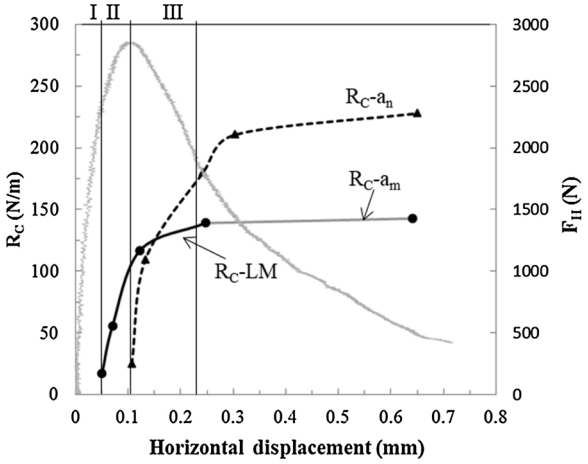

Fig. 9. Comparison of R_C behaviour determined by various methods (I: fracture initiation.
II: maximum load; III: onset of macro-crack).

According to Harmuth et al. [10,35], the stability of crack propagation and the material brittleness are related to the *R*-curve behaviour. The dependence of brittleness on the *R*-curve behaviour is given by:

$$l_{ch,\,max} = \pi a_0 \frac{K_M{}^2}{K_R{}^2}\left(1 + \frac{4}{W - 2a_0}\int_{a_0}^{\frac{W}{2}} \eta da\right) \tag{21}$$

where $l_{ch,max}$ is the upper limit for characteristic length, K_M the plateau value of the resistance against crack propagation, and K_R the resistance against crack initiation for the initial crack length a_o.

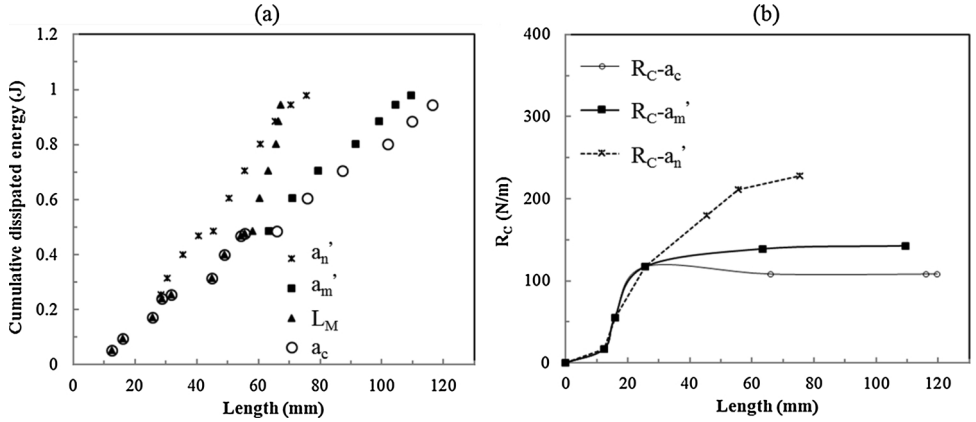

Fig. 8. Evolution of cumulative dissipated energy (a) and crack growth resistance R_C (b) with respect to crack lengths for magnesia spinel material.

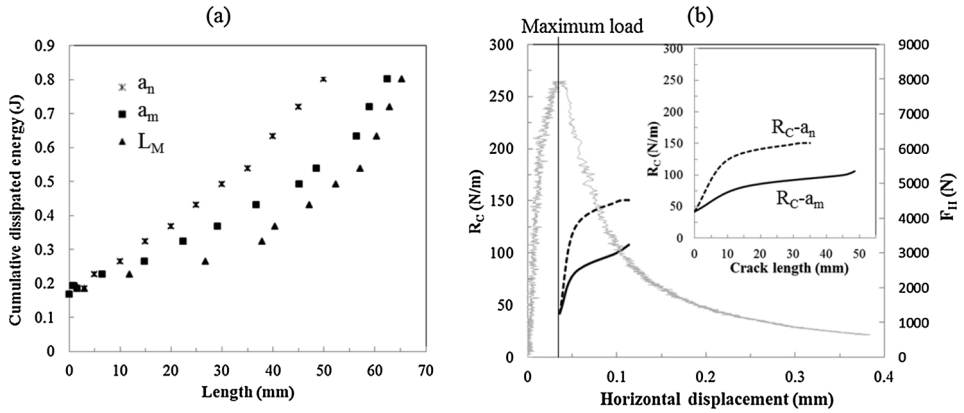

Fig. 10. Variation of the cumulative dissipated energy (a) and of the R_C (b) with respect to the crack lengths for magnesia material.

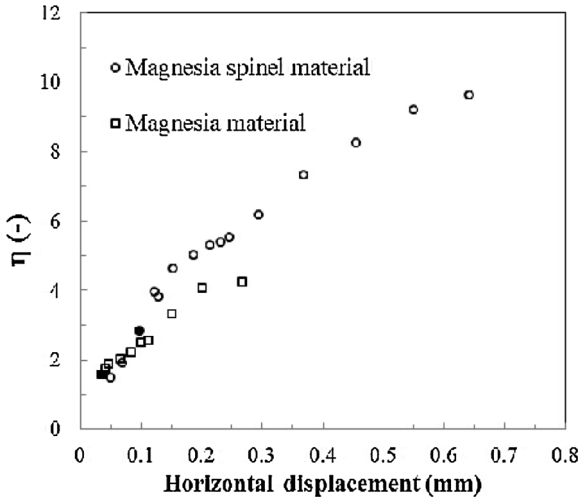

Fig. 11. Deviation from LEFM for magnesia spinel material and magnesia material as expressed by the quantity η (■ refers to load peak for magnesia material; ●refers to load peak for magnesia spinel material).

According to Eqs. (13) and (21), a high K_M/K_R ratio and a high η value contribute to the increase of the l_{ch}, which means a reduction of brittleness and increase of thermal shock resistance. As shown in Figs. 9 and 10, the magnesia spinel material exhibits a lower fracture initiation resistance while a higher crack propagation resistance compared with magnesia material. This corresponds to a low $K_R(a_0)$ value and a pronounced deviation from LEFM in the case of the magnesia spinel material. As expected, this higher deviation from LEFM is brought about by a larger FPZ formed during the fracture process of magnesia spinel material (indicated by the difference between localized zone length and macro-crack length). Fig. 11 represents quantity η, which has been evaluated according to Eqs. (13)–(16) for magnesia spinel material and magnesia material. For the magnesia material it is slightly higher when the horizontal displacement is smaller than 0.1 mm (before the load peak of magnesia spinel material). Therefore, in this region, the crack propagation of magnesia material and the FPZ development in magnesia spinel material show similar contribution to the deviation from LEFM. With the further enlarged FPZ and crack propagation, the magnesia spinel material exhibits a higher deviation from elasticity. At the final loading stage of both materials, η is more than twice for the magnesia spinel material compared with that of the magnesia material.

3.3. Comparison of R-curves determined by continuous and discontinuous loading

The loading–unloading technique is one of the most used approaches to investigate deviations from linear elastic fracture behaviour [14,36]. In this section, the difference of the loading–unloading technique and the universal dimensionless load–displacement diagram technique for determining the *R*-curve is discussed. The data acquired from loading–unloading technique used for comparison is published elsewhere [11]. The loading type of the loading–unloading technique is discontinuous as unloading steps are performed. Contrary, the universal dimensionless load–displacement diagram technique applies the load continuously. The crack propagation resistance is derived from the relation between the dissipated energy and the crack length. The dissipated energy is obtained respectively by using universal dimensionless load–displacement diagram technique (as shown in Fig. 2) and by loading–unloading technique. For both methods the composite crack length evaluated by DIC, which is the summation of the macro-crack length and localized zone length, is used to determine the crack propagation resistance. Seen from the Fig. 12(a), as the amount of loading–unloading cycles is limited, the number of data points of discontinuous loading technique is lower compared with that of the continuous loading. For the latter one R_C at each step of fracture process (i.e. fracture initiation, maximum load and the onset of macro-crack) is clearly shown in Fig. 12(b). For the loading–unloading technique the first loop is more like an average crack propagation resistance before the onset of macro-crack. Once the macro-crack is formed, R_C remains more or less constant and a plateau value is observed. It is higher for discontinuous loading compared to continuous loading. This is due to the friction of the crack faces causing some nonlinearity of the unloading and reloading path. Therefore, the dissipated energy for discontinuous loading method is higher for the same macro-crack extension (Fig. 12(a)). This implies the option of additional damage during the unloading-reloading process of the specimen.

Further a so-called superposition method is also an option to investigate the R_C behaviour of quasi-brittle material [14,37]. This approach has been adopted to investigate the *R*-curve behaviour of magnesia spinel material and magnesia material. Here, only a short discussion will be presented. A series of load–displacement curves of various specimens with different initial notch lengths was registered for further evaluation. The results have been considered to be not suitable to give representative results for brittleness reduced refractories and cannot be compared with the methods quoted above. This is due to the significance of the FPZ for the fracture behavior. If a crack of length $a > a_0$ has emerged a FPZ occurs behind (wake region) and in front of the crack tip (frontal process zone). This is not the case for an artificially introduced notch of same length a_0. Here the wake region is totally missing, and also the frontal process zone will only develop after further loading and crack propagation.

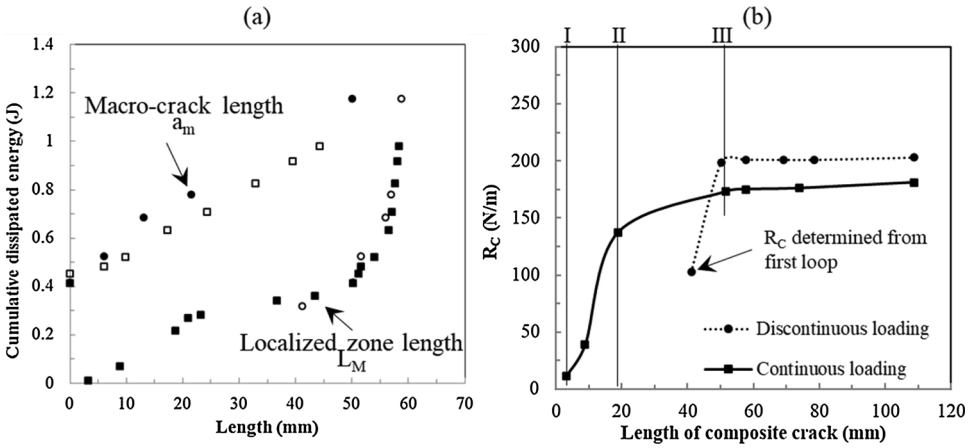

Fig. 12. Influence of the loading type on the determination of R_C (squares for continuous loading and circles for discontinuous loading) for a magnesia spinel refractory; meaning of I–III as in Fig. 9.

4. Conclusions

Due to the pre-existing micro-crack network in the virgin magnesia spinel material, the resistance for fracture initiation decreases compared with magnesia material. The crack propagation resistance of magnesia spinel material is higher than that of the magnesia material because of the formation of a sizable FPZ during the fracture process. Energy consuming processes occurring in the FPZ, such as the friction and grain bridging, avoid the decrease of the fracture energy for crack propagation by the low fracture energy for crack initiation. Furthermore, the ascending ratio of the crack propagation resistance to the fracture initiation resistance is favourable for the brittleness reduction and the good thermal shock resistance. The refractory material with reduced brittleness exhibits a significant deviation from LEFM.

Various methods for the determination of *R*-curves have been compared in this work. The universal dimensionless load–displacement diagram technique is particularly emphasized as an effective technique for evaluating of the *R*-curve behaviour of ordinary refractory ceramics. It requires a single specimen only and no artificial unloading step which may consume additional energy due to friction and imperfect match of the cracked faces. As the universal dimensionless load–displacement diagram method applies continuous loading, the irreversible energy dissipated at each loading stage can be evaluated and more data points are acquired. According to the state of the art, a nominal crack length was determined as function of compliance. However, with the application of the nominal crack length and the assumption of the crack initiation at peak load, the *R*-curve determined by the universal dimensionless load–displacement diagram technique may deviate from the actual material behaviour. Complementally, the DIC technique proved to show favourable applicability together with the universal dimensionless load–displacement diagram technique. With the application of DIC, the crack branching phenomenon and the development of micro-cracks were observed instantaneously. Thus, the crack tip can be precisely located. Instead of a straight crack path, the crack length is measured considering the crack tortuosity. For quasi-brittle materials, the fracture process consists of two main stages: the formation and propagation of FPZ and the following development of a macro-crack. The combination of DIC with the universal dimensionless load–displacement diagram technique allows to determine *R*-curves which better represent the actual fracture process occurring at different loading stages. The fracture starts in the pre-peak region for refractory material showing reduced brittleness according to the DIC observation. However, according to the state of the art, fracture initiation is assumed at maximum load for the universal dimensionless load–displacement diagram technique and the nominal crack length is defined by the compliance method. Then the determined fracture initiation resistance is actually representing the resistance of the FPZ extension. Once the macro-crack within the localized zone is onset, the further extension of FPZ is limited and the macro-crack is steadily propagating. The plateau of *R*-curve is corresponding with the fracture process at this fracture stage. Furthermore, the defined composite crack length allows to distinguish quantitatively the contribution of the extension of FPZ and of the propagation of macro-crack to the crack propagation resistance at second fracture stage.

Declaration of Competing Interest

The authors declare that they have no known competing financial interests or personal relationships that could have appeared to influence the work reported in this paper.

Acknowledgements

Financial support by the National Natural Science Foundation of China (Grant number: 51902228 and U1908227), the Provincial Natural Science Foundation of Hubei Province, China (Grant number: 2019CFB146), the Austrian Federal Government (in particular from Bundesministerium für Verkehr, Innovation und Technologie and Bundesministerium für Wissenschaft, Forschung und Wirtschaft) represented by Österreichische Forschungsförderungsgesellschaft mbH and the Styrian and the Tyrolean Provincial Government, represented by Steirische Wirtschaftsförderungsgesellschaft mbH and Standortagentur Tirol, within the framework of the COMET Funding Programme (K2 MPPE project A4.21) are gratefully acknowledged.

References

[1] R.C. Bradt, H. Harmuth, The fracture resistance of refractories, Refract. Worldforum 3 (4) (2011) 129–135.
[2] M. Sakai, Fracture mechanics of refractory materials, Taikabutsu Overseas 8 (2) (1988) 4–12.
[3] A.C. Mazzei, J.A. Rodrigues, V.C. Pandolfelli, Alumina-mullite-zirconia composites obtained by reaction sintering Part II. R-Curve behavior, J. Mater. Sci. 35 (11) (2000) 2815–2824.
[4] H. Harmuth, K. Rieder, M. Krobath, E. Tschegg, Investigation of the nonlinear fracture behaviour of ordinary ceramic refractory materials, Mater. Sci. Eng., A 214 (1) (1996) 53–61.
[5] R. Grasset-Bourdel, A. Alzina, M. Huger, T. Chotard, R. Emler, D. Gruber, H. Harmuth, Tensile behaviour of magnesia-spinel refractories: comparison of tensile and wedge splitting tests, J. Eur. Ceram. Soc. 33 (5) (2013) 913–923.
[6] D.P.H. Hasselman, Unified theory of thermal shock fracture initiation and crack propagation in brittle ceramics, J. Am. Ceram. Soc. 52 (11) (1969) 600–604.
[7] A. Hillerborg, M. Modéer, P.E. Petersson, Analysis of crack formation and crack growth in concrete by means of fracture mechanics and finite elements, Cem. Concr. Res. 6 (6) (1976) 773–781.
[8] D. Gruber, M. Sistaninia, C. Fasching, O. Kolednik, Thermal shock resistance of

magnesia spinel refractories—investigation with the concept of configurational forces, J. Eur. Ceram. Soc. 36 (16) (2016) 4301–4308.
[9] C. Aksel, P.D. Warren, Thermal shock parameters [R, R‴ and R⁗] of magnesia–spinel composites, J. Eur. Ceram. Soc. 23 (2) (2003) 301–308.
[10] H. Harmuth, E.K. Tschegg, A fracture mechanics approach for the development of refractory materials with reduced brittleness, Fatigue Fract. Eng. Mater. Struct. 20 (11) (1997) 1585–1603.
[11] Y. Dai, D. Gruber, H. Harmuth, Determination of the fracture behaviour of MgO-refractories using multi-cycle wedge splitting test and digital image correlation, J. Eur. Ceram. Soc. 37 (15) (2017) 5035–5043.
[12] E.K. Tschegg, K.T. Fendt, C. Manhart, H. Harmuth, Uniaxial and biaxial fracture behaviour of refractory materials, Eng. Fract. Mech. 76 (14) (2009) 2249–2259.
[13] R. Gettu, Z.P. Bazant, M.E. Karr, Fracture properties and brittleness of high-strength concrete, Mater. J. 87 (6) (1990) 608–618.
[14] M. Sakai, R.C. Bradt, Graphical methods for determining the nonlinear fracture parameters of silica and graphite refractory composites, in: R.C. Bradt (Ed.), Fracture Mechanics of Ceramics, 7 Springer, New York, NY, USA, 1986, pp. 127–142.
[15] D.M. Tan, K. Rieder, Determination of R-curves of ordinary refractory ceramics from measurements of a new wedge splitting test method, Fortschrittsberichte der Deutschen Keramischen Gesellschaft (Germany) 10 (3) (1994) 71–76.
[16] D.M. Tan, E.K. Tschegg, S.E. Tschegg-Stanzl, Fracture mechanical characterization of asphalt aggregate mixtures at different temperatures, in: M.H. Alisbadi (Ed.), Localized Damage III, Computer-Aided Assessment and Control, Computational Mechanics Publications, Southampton, U.K, 1994, pp. 217–224.
[17] Y. Dai, D. Gruber, H. Harmuth, Observation and quantification of the fracture process zone for two magnesia refractories with different brittleness, J. Eur. Ceram. Soc. 37 (6) (2017) 2521–2529.
[18] Ł. Skarżyński, J. Tejchman, Experimental investigations of fracture process using DIC in plain and reinforced concrete beams under bending, Strain 49 (6) (2013) 521–543.
[19] J. Tejchman, J. Bobiński, Continuous and Discontinuous Modelling of Fracture in Concrete Using FEM, Springer Science & Business Media, New York, NY, USA, 2012.
[20] Y. Dai, Y. Li, S. Jin, Y. Li, H. Harmuth, X. Xu, Mechanical and fracture investigation of magnesia refractories with acoustic emission-based method, J. Eur. Ceram. Soc. 40 (1) (2020) 181–191.
[21] H. Harmuth, R.C. Bradt, Investigation of refractory brittleness by fracture mechanical and fractographic methods, Int. Ceram. Rev. 62 (4) (2010) 264–269.
[22] D. Ewest, P. Almroth, B. Sjödin, K. Simonsson, D. Leidermark, J. Moverare, A modified compliance method for fatigue crack propagation applied on a single edge notch specimen, Int. J. Fatigue 92 (2016) 61–70.
[23] V. Veselý, P. Konečný, P. Lehner, Influence of crack propagation on electrical resistivity and ultrasonic characteristics of normal concrete assessed by sequential TPB fracture test, Theor. Appl. Fract. Mech. 80 (2015) 2–13.
[24] R.P. Gangloff, Electrical potential monitoring of crack formation and subcritical growth from small defects, Fatigue Eng. Mater. Struct. 4 (1) (1981) 15–31.
[25] Z. Wu, H. Rong, J. Zheng, F. Xu, W. Dong, An experimental investigation on the FPZ properties in concrete using digital image correlation technique, Eng. Fract. Mech. 78 (17) (2011) 2978–2990.
[26] Y. Wang, P. Lava, S. Coppieters, M. De Strycker, P. Van Houtte, D. Debruyne, Investigation of the uncertainty of DIC under heterogeneous strain states with numerical tests, Strain 48 (6) (2012) 453–462.
[27] F. Mathieu, F. Hild, S. Roux, Identification of a crack propagation law by digital image correlation, Int. J. Fatigue 36 (1) (2012) 146–154.
[28] F. Hou, S. Hong, Characterization of R-curve behavior of translaminar crack growth in cross-ply composite laminates using digital image correlation, Eng. Fract. Mech. 117 (2014) 51–70.
[29] R. Vargas, J. Neggers, R.B. Canto, J.A. Rodrigues, F. Hild, Analysis of wedge splitting test on refractory castable via integrated DIC, J. Eur. Ceram. Soc. 36 (16) (2016) 4309–4317.
[30] E.K. Tschegg, Equipment and Appropriate Specimen Shape for Tests to Measure Fracture Values, Patent AT-390328 (1986).
[31] A.A. Griffith, The phenomena of rupture and flow in solids, Philos. Trans. R. Soc. London, Ser. A 221 (1921) 163–198.
[32] T. Fett, D. Munz, Stress Intensity Factors and Weight Functions 1 Computational Mechanics Publications, Southampton, U.K, 1997.
[33] G.R. Irwin, Analysis of stresses and strains near the end of a crack traversing a plate, J. Appl. Mech. 24 (3) (1957) 361–364.
[34] M. Sakai, R.C. Bradt, Fracture toughness testing of brittle materials, Int. Mater. Rev. 38 (2) (1993) 53–78.
[35] H. Harmuth, Stability of crack propagation associated with fracture energy determined by wedge splitting specimen, Theor. Appl. Fract. Mech. 23 (1) (1995) 103–108.
[36] B.J. Pease, J. Skocek, M.R. Geiker, J. Weiss, H. Stang, The wedge splitting test: influence of aggregate size and water-to-cement ratio, RILEM Transp. Mech. Cracked Concr. (2007) 111–122.
[37] V.C. Li, R.J. Ward, A novel testing technique for post-peak tensile behavior of cementitious materials, in: H. Mihashi (Ed.), Fracture Toughness and Fracture Energy: Test Methods for Concrete Rock, Leiden, The Netherlands, 1989, pp. 183–195.